Journal of Molecular Structure 1235 (2021) 130135

Contents lists available at ScienceDirect

Journal of Molecular Structure

journal homepage: www.elsevier.com/locate/molstr

Physicochemical and X-ray crystallographic properties of the first rhenium compound of benzophenone thiosemicarbazone (bptsc), *fac*-[Re(CO)$_3$(κ^2-N$_{im}$,S-bptsc)Cl]

Mohammed Bakir[a,*], Mark A.W. Lawrence[a], Junior Johnson[a], Colin McMillen[b]

[a] Department of Chemistry, University of the West Indies, Mona Kingston 7, Jamaica, West Indies
[b] Department of Chemistry, Clemson University, 379 Hunter Laboratories, Clemson, SC29634-0973, United States

ARTICLE INFO

Article history:
Received 13 December 2020
Revised 12 February 2021
Accepted 16 February 2021
Available online 25 February 2021

Keywords:
Rhenium
Benzophenone thiosemicarbazone
X-ray crystallography
Spectroscopy
DFT calculations
Electrochemistry

ABSTRACT

fac-[Re(CO)$_3$(κ^2-N$_{im}$,S-bptsc)Cl] (**2**), isolated from the reaction between Re(CO)$_5$Cl and benzophenone thiosemicarbazone, bptsc, (**1**) in refluxing toluene in air, is the first Re compound of **1** and is the second Re(CO)$_3$Cl compound of κ^2-N$_{im}$,S-coordinated ligand (im = imine). The authenticity of **2** was established from the results of its elemental composition, spectroscopic measurements, and X-ray crystallographic analysis. Single crystals of **2** grown from DMF are in the monoclinic space group $P2_1/c$. The asymmetric unit of **2** revealed pseudo-octahedral coordination about Re. Two carbonyl C atoms, an imine N atom and a thione S atom occupy the equatorial sites and the axial sites are occupied by a carbonyl C atom and a Cl atom. The κ^2-N,S-coordination of **1** to Re forms a semi-planar five-membered [Re-N-N–C-S] metallocyclic ring. The extended structure disclosed stacks of molecules interlocked via a web of N–H···X (*X* = Cl or O), S···S and C–H···π interactions. DFT calculations divulged facile delocalization of electron density in the molecule and interatomic distances and angles in good agreement with the solid state structure. Electrochemical measurements on **2** in CH$_3$CN and DMF revealed sequential irreversible electron transfers pointing to structural changes due to electrochemically induced thione-thiol tautomerization of the thioamide moiety. Plausible mechanisms for the oxidative and reductive electrochemical decomposition of **1** and **2** are reported. The proposed mechanisms are in good agreement with those reported in the literature for closely related compounds.

1. Introduction

Benzophenone thiosemicarbazone, bptsc, (**1**) (see Scheme 1) and its derivatives have attracted research interest for their convenient synthesis [1,2], physicochemical properties [3–8] and implications in many important processes [1,7,9–12]. The non-linear optical (NLO) behavior of **1** revealed efficient semiconducting properties [13,14]. The NLO activity of **1** is due in part to the donor-accepting capacity of the benzophenone to thiosemicarbazone. The thione (C=S) moiety enhances the second harmonic generation (SHG) efficiency. Catalytic Suzuki-Miyaura C–C and C–N cross coupling reactions were induced by an orthometallated Pd-complex of **1** and closely related complexes [7]. Benzophenone thiosemicarbazones were utilized as sensitive analytical reagents for the detection and determination of trace amounts of hazardous metal ions such as Cd(II) and Hg(II) in drinking water [10,15,16]. The agronomical [1], and medicinal [9,17] application of **1** were investigated and revealed interesting antiflatoxigenic [1], anti-fungal [12] and antitumor [9,11,12,17] properties. The chelating properties of benzophenone thiosemicarbazones account in part for their environmental, and biological applications.

Although physicochemical properties and biological implications of variety of metal compounds of **1** were reported, there has been no report on the chemistry of **1** with high- or low-valent rhenium compounds. This study describes the synthesis, spectroscopic, solid state structure, DFT calculations and electrochemical properties of the first rhenium compound of **1**, *fac*-[Re(CO)$_3$(κ^2-N$_{im}$,S-bptsc)Cl] (**2**) (see Scheme 1). This is in continuation of our efforts to explore the chemistry of hydrazonic compounds of the type [R$_1$R$_2$C=N–NH-(*C*=*X*)$_n$Y] (R$_1$ and R$_2$ = aryl, heterocyclic; n = 0 or 1 with *Y* = alkyl, aryl or heterocyclic (hydrazone); n = 1 with *Y* = NH$_2$ or NR$_1$R$_2$ and X = O (semicarbazone) and X = S (thiosemicarbazone) [18–21]. Our interest in the chemistry of hydrazonic compounds stems from their diverse reactivity patterns,

* Corresponding author.
E-mail address: mohammed.bakir@uwimona.edu.jm (M. Bakir).

https://doi.org/10.1016/j.molstruc.2021.130135
0022-2860/

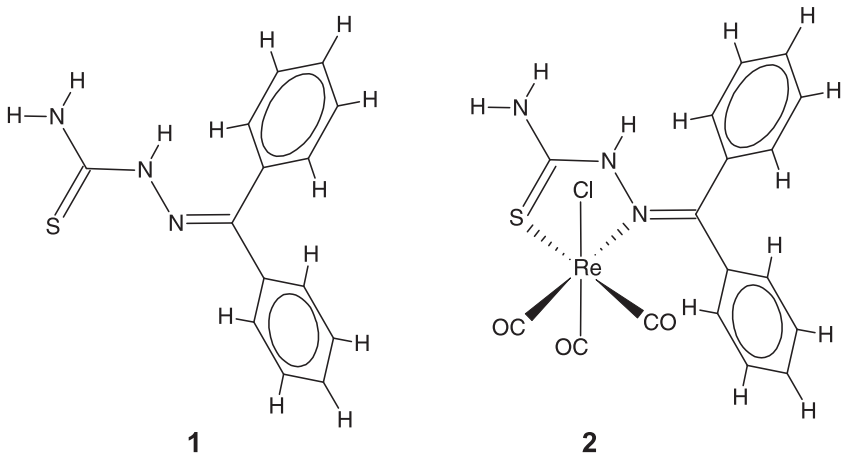

Scheme 1. Representations of bptsc (**1**) and *fac*-[Re(CO)$_3$(κ^2-N$_{im}$,S-bptsc)Cl] (**2**).

rich physicochemical properties, and molecular sensing and catalytic behavior.

2. Experimental

2.1. Reagents

Re(CO)$_5$Cl was purchased from Strem Chemicals, Inc.; benzophenone (bp) and thiosemicarbazide (tsc) were purchased from Sigma-Aldrich. All other reagents were obtained from commercial sources and used as received. **1** was prepared from the acid catalyzed condensation of benzophenone (bp) with thiosemicarbazide (tsc) in refluxing acidified ethanol in air as described in the literature [1]. Anal. Calcd. for $C_{14}H_{13}N_3O$ (%): C, 65.85; H, 5.13; N, 16.46. Found: C, 65.80; H, 5.00; N, 16.78. Selected IR (KBr disk, cm^{-1}): ν(NH$_2$) 3430, 3345 (s), ν(N–H) 3257 (broad), ν(C=N) + ν(C=C) 1610 and 1477, ν(C=S) + ν(N–C-N) 1083, 1070, ν(C=S) 846. UV–visible / nm ($\varepsilon \pm 300$ / cm^{-1}M^{-1}) in CH$_3$CN: 315 (16,200), in DMF: 319 (17,700). ^{1}H NMR (δ, ppm) in DMSO-d_6: 8.67 (s, 1H, NH), 8.40 (s, 2H, NH$_2$), 7.67–7.63 (m, 5H, aromatic) and 7.42–7.34 (m, 5H, aromatic). ^{13}C NMR (δ, ppm): 177.7, 149.1, 136.3, 131.2, 130.0, 129.8, 129.7, 128.3, 128.2, 127.6.

2.2. Synthesis of fac-[Re(CO)$_3$(κ^2-N$_{im}$, S-bptsc)Cl] (2)

A mixture of Re(CO)$_5$Cl (160 mg, 0.39 mmol), **1** (99 mg, 0.39 mmol), and toluene (30 mL) was refluxed for 4 h. Slow evaporation of the mixture gave a yellow powder that was filtered off, washed with CH$_3$CN and dried. Yield 190 mg (87%). Anal. Calcd. for $C_{17}H_{13}ClN_3O_3ReS$ (%): C, 36.39; H, 2.34; N, 7.49. Found: C, 36.56; H, 2.13; N, 7.22. Selected IR (KBr disk, cm^{-1}): ν(NH$_2$) 3436, 3264 (s), ν(NH) 3180 (s), ν(C=N) 1614, ν(C≡O) 1887, 1945, and 2026 (vs), ν(C=N) + ν(C=C) 1698, 1614, 1563, 1556 and 1428, ν(C=S) + ν(N–C-N) 1176 and 1170 and ν(C=S) 798. UV-visible /nm ($\varepsilon \pm 300$/ M^{-1}cm^{-1}) in DMF: 319 (11,950), 356 sh (5600). ^{1}H NMR (δ, ppm) in DMSO-d_6: 11.65 (s, 1H), 9.26 (s, 1H), 8.26 (s, 1H), 7.60–7.41 (m, 10 H). ^{13}C NMR (δ, ppm): 196.8, 193.9, 190.6, 179.8, 169.2, 140.3, 134.3, 131.7, 130.2, 129.5, 129.1, 128.4, 128.3, 127.5.

2.3. Physical measurements

Electronic absorption spectra were recorded on a HP8543 diode array spectrometer. Solution ^{1}H and ^{13}C NMR spectra were recorded on a Bruker ACE 500-MHz Fourier-transform spectrometer and referenced to the residual protons in the incompletely deuterated solvent. Infrared spectra were recorded as KBr pellets on a Bruker Vector 22 FT-IR Spectrometer.

Electrochemical measurements were performed with the use of a DigiIvy DY2312 potentiostat, under an argon atmosphere at room temperature, and were uncorrected for junction potential. A standard three electrode cell setup was employed, using a glassy carbon working electrode (diameter = 3 mm), Ag wire quasi-reference electrode (QRE) and Pt wire as an auxiliary electrode; against which Fe(Cp)$_2$/Fe(Cp)$_2^+$ couple appeared at $E_{1/2}$ = +0.65 V in DMF and $E_{1/2}$ = +0.48 V in CH$_3$CN. Solvents used in the electrochemical experiments were dried using standard procedures [22].

2.4. DFT calculations

Density functional theory (DFT) calculations were carried out on **2** in the gas phase and in DMF using the GAMESS software package[1] [23,24]. The structure was optimized in the gas phase as indicated by the absence of imaginary frequencies in the Hessian, using PW91X/SBKJC [25,26] with the common polarization and spherical coordinates. Solvent optimization in DMF was carried out using the SMD solvation method [27]. The GAMESS input file was generated using MacMolPlt 7.7[2] [28], and the output file viewed using the same. The bond angles and lengths of the optimized structure (see Supplemental Table 1) are comparable to those obtained from X-ray structural analysis suggesting that the basis sets employed are satisfactory. The SBKJC basis set results was initially compared to those obtained using the improved model core potentials with scalar relativistic effects (PW91X/IMCP-SR2) [29,30]. This basis set provided comparable FMO to the SBKJC basis set, albeit with different energies (as was expected, see supporting information). The PW91X/SBKJC level of theory was adopted since it gave reasonable values relative to the experimental values without the computational expense.

2.5. Crystal structure of fac-[Re(CO)$_3$(κ^2-N$_{im}$, S-bptsc)Cl] (2)

Single crystals of **2** were grown from DMF when allowed to stand in air for several days. X-ray diffraction data were collected on a yellow columnar crystal. A Bruker D8 Venture diffractometer having a Mo (λ = 0.71073 Å) microfocus source and a Photon 100 detector were used for data collection. Data were processed and corrected for absorption using multi-scan techniques (SADABS). The structure was solved by intrinsic phasing (SHELXT), and

[1] GAMESS: an open-sourcegeneral ab initio quantum chemistry package. https://www.msg.chem.iastate.edu/gamess/index.html

[2] MacMolPlt: an open-source molecular builder and visualization tool for GAMESS. http://brettbode.github.io/wxmacmolplt/

Table 1
Crystal data and structure refinement for *fac*-[Re(CO)$_3$(κ^2-N$_{im}$,S-bptsc)Cl] (**2**).

Empirical formula	$C_{17}H_{13}ClN_3O_3ReS$
F. W. (g/mol)	561.01
Temperature (K)	173(2)
Crystal system	Monoclinic
Space group	$P2_1/c$
a (Å)	6.5396(7)
b (Å)	17.9807(18)
c (Å)	16.1311(16)
β (°)	97.573(4)
Volume (Å^3)	1880.3(3)
Z	4
D(calcd)(g/cm^3)	1.982
μ, mm^{-1}	6.737
F(000)	1072
Crystal size (mm)	0.03 × 0.03 × 0.19
θ range,°	2.60 to 25.50
Reflections collected	40,273
Indep. Reflections	3490 [R(int) = 0.0518]
Limiting indices	−7←h→7, −21←k→21; −19←l→19
Goodness of fit (S)	1.279
No. of parameters	244
R indices (I>2σ(I))	R_1[a] = 0.0488, wR_2[b] = 0.1011[†]
R indices (all data)	R_1[a] = 0.0536, wR_2[b] = 0.1028
Largest diff. peak and hole (e.Å^3)	2.446 and −3.418
CCDC No.	1,986,270

[†] [a]$R_1 = S||F_o| - |F_c||/S|F_o|$ and [b]$wR_2 = \{S[w(F_o^2 - F_c^2)^2]/S[wF_o^2]^2\}^{1/2}$.

refined by full matrix least squares on F^2 (SHELXL) [31]. All non-hydrogen atoms were refined anisotropically. H atoms attached to C atoms were refined in calculated positions using riding models. H atoms attached to N atoms were located from difference electron density maps and their positions refined. In the final refinement cycle, seven peaks greater than 1 e Å^{-3} appeared in the difference map. Six of these surround Re and can be attributed to residual effects of absorption. One peak was at 1.997 Å from C16 and has no chemical significance. Cell parameters and other crystallographic information are given in Table 1 and the supporting crystallographic files (CIF) (Table 2).

3. Results and discussion

3.1. Synthesis and characterization

Following a procedure similar to those reported for the synthesis of variety of *fac*-Re(CO)$_3$Cl compounds of α-diimine, di-2-pyridyl ketone hydrazonic compounds and closely related ligands, *fac*-[Re(CO)$_3$(κ^2-N$_{im}$,S-bptsc)Cl] (**2**) was isolated in good yield (87%) from the reaction between Re(CO)$_5$Cl and **1** in refluxing toluene in air [21,32]. The identity of **2** was established from the results of its elemental analysis and a number of spectroscopic measurements, and confirmed from the results of single crystal X-ray crystallography. In the infrared spectra of **2**, peaks appeared in the ν(NH$_2$), ν(NH), ν(CH), ν(C≡O), combine ν(C=N) + ν(C=C), combined ν(C=S) + ν(N-C-N) and ν(C=S) (see experimental section) consistent with the coordination of **1** to *fac*-Re(CO)$_3$Cl. Three peaks appeared in the carbonyl ν(C≡O) region similar to those reported for variety of *fac*-[Re(CO)$_3$(κ^2-L-L)Cl] (L-L = N,N-bidentate ligand) [33–35]. Comparison of the spectrum of **2** with that of **1** shows changes in the combined ν(C=N) + ν(C=C) between 1650 – 1400 cm^{-1}, combined ν(C=S) + ν(N–C-N) between 1200 – 1000 cm^{-1}, and ν(C=S) between 850 – 800 cm^{-1} [36] (see experimental section) consistent with κ^2-N,S-coordination of **1**.

^{1}H and ^{13}C NMR measurements on DMSO-d_6 solutions of **1** and **2** confirmed the κ^2-N$_{im}$,S-coordination of **1** to *fac*-Re(CO)$_3$Cl moiety via the S atom of the thioimide, and the N atom of the imine (C=N) group. This is evident from the downfield shift of the amide (NH) proton as well as the thione (C=S) and imine (C=N) C resonances of **2** compared to **1** (see experimental section). The downfield shift of the NH proton points to the increase in its acidity due to κ^2-N$_{im}$,S-coordination of **1** to Re. The significant downfield shift of the imine (C=N) C atom confirms the imine coordination of **1**. In the ^{13}C NMR spectrum of **2**, the thione (C=S) and imine (C=N) C resonances appeared at 179.8 and 169.2 ppm, while in **1** these resonances appeared at 177.7 and 149.1 ppm. The slight downfield shift of the thioamide (C=S) C resonance and significant downfield shift of the imine (C=N) C resonance of **2** compared to **1** point to stronger binding of the imine N atom to *fac*-Re(CO)$_3$Cl moiety. The terminal amino (NH$_2$) protons of **2** are not equivalent, appeared at 9.24 and 8.25 ppm upfield from the 11.65 ppm of the thioamide NH proton resonance. In the case of **1,** the terminal amine protons are equivalent, appeared as a singlet at 8.40 ppm upfield from the 8.67 ppm singlet of the thioamide NH proton. The aromatic protons of **2** coalesce pointing to higher symmetry due to binding of **1** to Re compared to the aromatic protons of **1**.

3.2. Solid state structure

Crystals of **2** grown from DMF are in the centrosymmetric monoclinic space group $P2_1/c$. The asymmetric unit of **2** is shown in Fig. 1. The coordination about Re is pseudo-octahedral with an imine N atom, a thione S atom and two carbonyl C atoms occupy the equatorial positions, and the axial positions are occupied by a carbonyl C atom and a Cl atom.

Deviation from idealized octahedral geometry is due to κ^2-N$_{im}$,S-binding of **1**. This is evident from the N1-Re1-S1, N1-Re1-Cl1 and C2-Re1-Cl1 bond angles of 79.98(19)°, 79.05(19)° and 174.7(3)°, respectively. The κ^2-N$_{im}$,S-binding of **1** to Re forms a virtually planar five-membered [-Re1-N3-N2-C4-S1-] metallocyclic ring as evident from the Re1-S1-C5-N2 and C5-N2-N1-Re1 dihedral angles of +5.0(8) and +8.0(10)°, respectively. The thiosemicarbazone C5-N1-N2-C4 moiety with dihedral angle of +171.4(8)° is nearly planar. The phenyl rings are neither co-planar to each other nor to the thiosemicarbazone backbone as evident from C11-C4-C21-C22, C21-C4-C11-C12 and N1-C4-C11-C12 dihedral angles of −52.9(1), +127.9(9) and −51.4(12)°. The C=S bond distance of 1.698(9) Å is of the same order as the 1.6866(17) Å and 1.680(1) Å of uncoordinated **1** and H2htp [1-(1–2-hydroxyphenyl)ethylidene)-4-phenylthiosemicarbazone], respectively [30]. The Re1-N1 and Re1-S1 bond lengths of 2.228(7) and 2.470(2) Å are similar to the 2.242(3) and 2.467(1) Å bond distances reported for the imine (Re-N) and thione (Re-S) coordinated H2htp in *fac*-[Re(CO)$_3$(κ^2-N$_{im}$,S-

Table 2
Hydrogen bond distances (Å) and angles (°) for **2.**

D-H···A	d(D-H)	d(H···A)	d(D···A)	<(DHA)	Symmetry Transformation
N3-H3A···Cl1	0.90(7)	2.48(8)	3.308(9)	152(9)	x-1, y, z
N3-H3B···O1	0.84(7)	2.29(8)	3.122(11)	167(11)	-x + 1, -y, -z + 1
N2-H2···Cl1	0.84(7)	2.39(8)	3.138(7)	148(9)	x-1, y, z
Non-covalent interactions					
S···S	D(S···S) = 3.385 Å				
C22-H22···π	d(C-H···centroid) = 3.051 Å			<C-H···centroid = 145.04°	

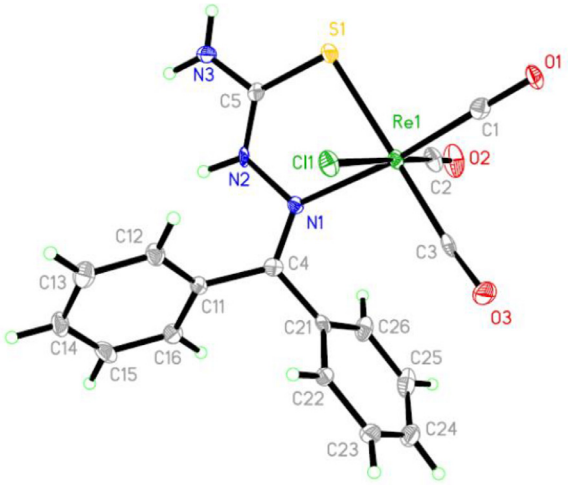

Fig. 1. A view of the structure of **2** with displacement ellipsoids drawn at the 30% probability level. H atoms are shown as isotropic spheres of arbitrary radius.

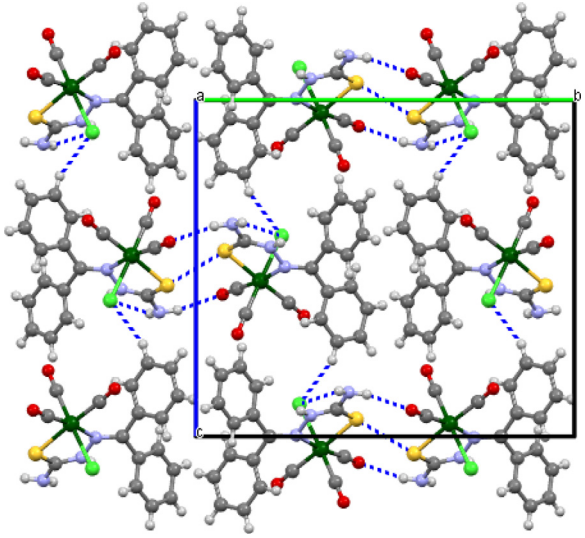

Fig. 3. Packing of molecules in **2**, viewed along the a-axis. N–H···O, N–H···Cl, C–H···Cl, and S···S interactions are shown as blue dashed lines.

H2htp)(κ^1-S-H2htpi)Cl] (H2htpi is the thiolate-iminium zwitterionic H2htp) [37]. The Re1-S1 bond length in **2** is slightly shorter than the 2.536(1) Å Re-S distance of monodentate coordinated κ^1-S-H2htpi in *fac*-[Re(CO)$_3$(κ^2-N$_{im}$,S-H2htp)(κ^1-S-H2htpi)Cl]. The average Re-C bond distance of 1.913(10) Å is normal and of the same order as those reported for *fac*-[Re(CO)$_3$(κ^2-N,N-L-L)Cl] compounds [37–39].

Classical hydrogen bonds of the type N–H···X (X=O or Cl) and non-covalent S···S interaction, and C–H···π interactions link adjacent molecules in the extended structure (see Table 3, Fig. 2). The packing of molecules revealed stacks of **2** linked via a web of non-covalent interactions (see Fig. 3). The bond distances and angles of the classical hydrogen bonds are normal and similar to those reported for variety of N–H···X hydrogen bonds [39].

3.3. DFT calculations

Fig. 4 shows the frontier molecular orbitals of **2** in the gas phase and in DMF. The calculated ν(NH$_2$) appeared at 3400 and 3295 cm^{-1} while ν(NH) appeared at 3014 cm^{-1}. These values are similar to the 3436, 3264 and 3180 cm^{-1} observed in the infrared spectra of **2**. The calculated ν(C≡O) appeared at 2013, 1941, and 1921 cm^{-1} while the infrared spectra showed three peaks at 2026, 1945, and 1887 cm^{-1}. The slight variation between the calculated and experimental values are due to solid state effect. The bond lengths and angles are of the same order as those obtained from X-ray structural analysis (see supplementary Table S1). The frontier MOs of the LUMO are scattered across the phenyl rings, *fac*-Re(CO)$_3$ and hydrazone backbone and the LUMO(+) MOs are scattered over a phenyl ring, hydrazone backbone and the carbonyl groups in the gas phase. The solvated model shows the LUMO MOs involve the phenyl rings and the hydrazone backbone while the LUMO+1 MOs scatter across the hydrazone backbone, and *fac*-Re(CO)$_3$. The key feature in the electronic spectrum of **2** is the overlap between π-π^* transition of the ligand with the MLCT transition at ~ 300 nm (Fig. S1). A shoulder due to MLCT transtion at ~ 356 nm is partially resolved from the ligand transition. TDHF analysis of the singlet excited states consists primarily of transitions from the HOMO to LUMO+n (n = 1 to 10) of which the HOMO to LUMO+4 and +5 are the most intense (with oscillator strengths

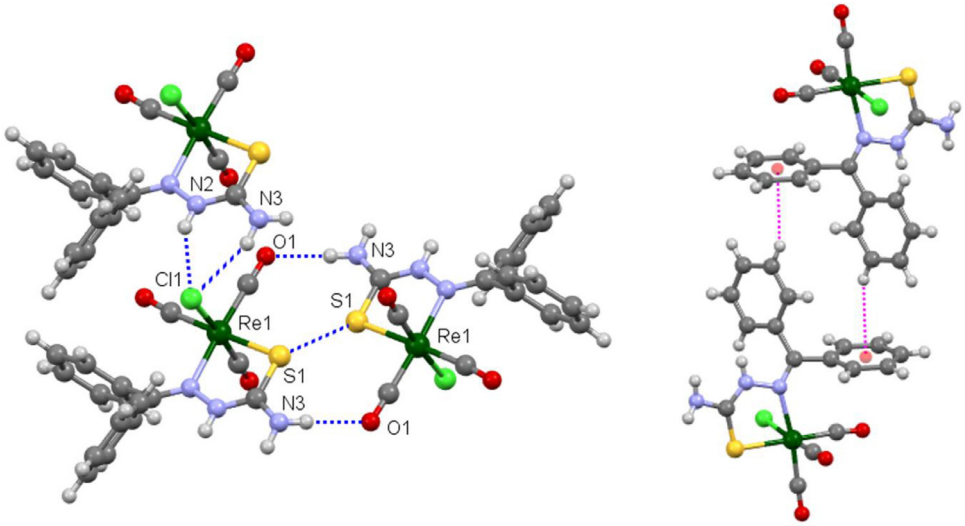

Fig. 2. Intermolecular interactions in 2. Classical hydrogen bonds are shown on the left (blue dashed contacts) and C–H···π interactions are shown on the right (magenta dashed contacts)

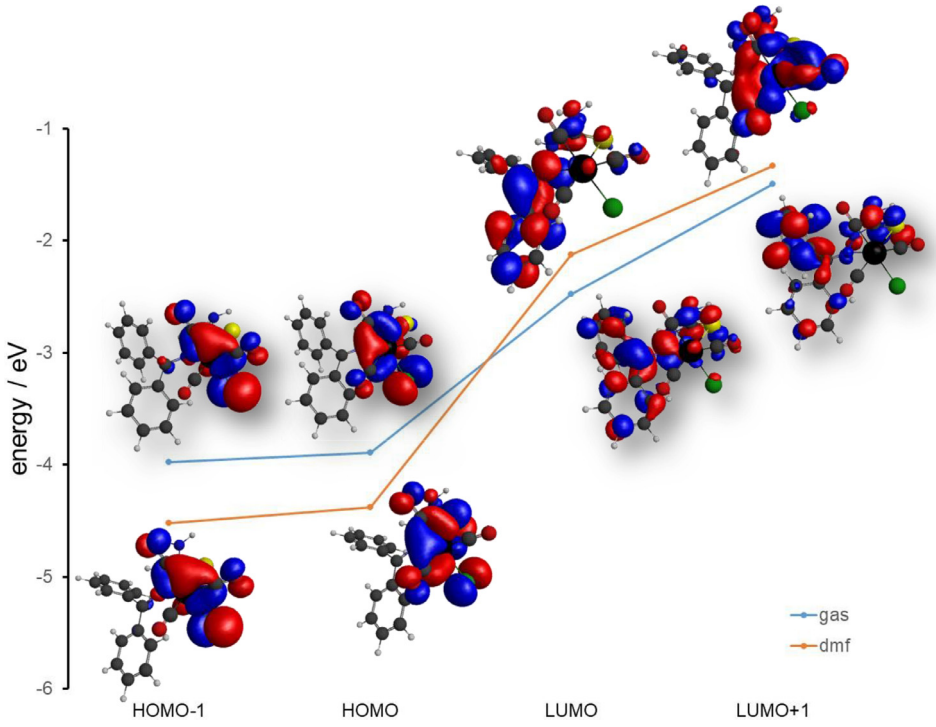

Fig. 4. DFT optimized structures in the gas phase (PW91X/SBKJC, shadowed images) and in DMF (PW91X/SBKJC/SMD) for **2**.

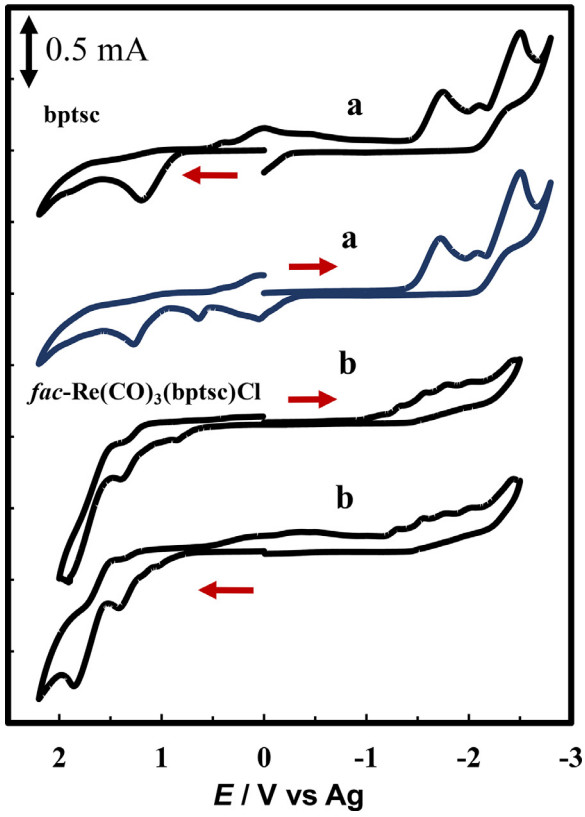

Fig. 5. Cyclic voltammograms of CH_3CN solutions containing 0.1 M $[^nBu_4N]PF_6$ of 14 mM **1 (a)** and 12 mM **2 (b)** at a glassy carbon working electrode (dia = 3.0 mm) vs Ag.

of 0.2719 and 0.2493, respectively). The frontier MOs suggest that the observed transitions are indeed π-π^* transition of the ligand mixed with MLCT of Re. The two most intense singlet transitions predicted to occur at 251 and 252 nm due to Re→phenyl and Re→NHC=S moieties are masked by DMF (see Supporting information). The MLCT transition due to the carbonyl moieties, observed at 319 nm (in DMF) is predicted to occur at 290 nm. The ~ 30 nm difference between the observed and the calculated bands is the result of TDHF singlet excited states being calculated in the gas phase. It is known that the π^* orbitals of carbonyl will interact with the polar solvent which will lower the orbital energies.

3.4. Electrochemical properties

Electrochemical measurements on **1** and **2** in CH_3CN and DMF were investigated using voltammetric techniques. Fig. 5 shows cyclic voltammograms of **1** and **2** measured in CH_3CN.

The voltammograms display irreversible redox processes on oxidatively and reductively initiated scans signifying structural changes following electronic transfer. Reductively initiated scan on **1** (Fig. 5a) shows irreversible reductions at $E_{p,c}$ = −1.65, −2.10 and −2.50 V followed by electrochemically generated product waves at $E_{p,a}$ = +0.02, +0.60 V due to the oxidation of the reductively generated product waves (see Scheme 2) along with an irreversible oxidation at $E_{p,a}$ = +1.20 V. On oxidatively initiated scan (Fig. 5a), the reductively generated product waves disappeared and oxidatively generated product waves appeared at $E_{p,c}$ = +0.35, +0.04 and −0.42 V. The electrochemical signature of **1** in DMF is similar to that observed in CH_3CN along with additional oxidation waves appeared between $E_{p,a}$ = +1.30 to +2.00 V (see Figure S4). The results point to facile electrochemical decomposition of **1** in CH_3CN and DMF. The voltammograms of **1** are similar to those of di-2-heteroaromatic hydrazonic compounds that include di-2-pyridyl ketone hydrazones, di-2-pyridyl ketone thiosemicarbazone and di-2-thienyl ketone thiosemicarbazone. Plausible mechanisms for the oxidative and reductive decomposition of **1** are shown in Scheme 2.

The voltammogram of **2** measured in CH_3CN on reductively initiated scan (Fig. 5b) displays a series of a closely spaced irreversible reductions at $E_{p,c}$ = −1.30, −1.55, −1.80, −2.00 V and an irreversible reduction at $E_{p,c}$ = −2.40 V. The voltammogram also

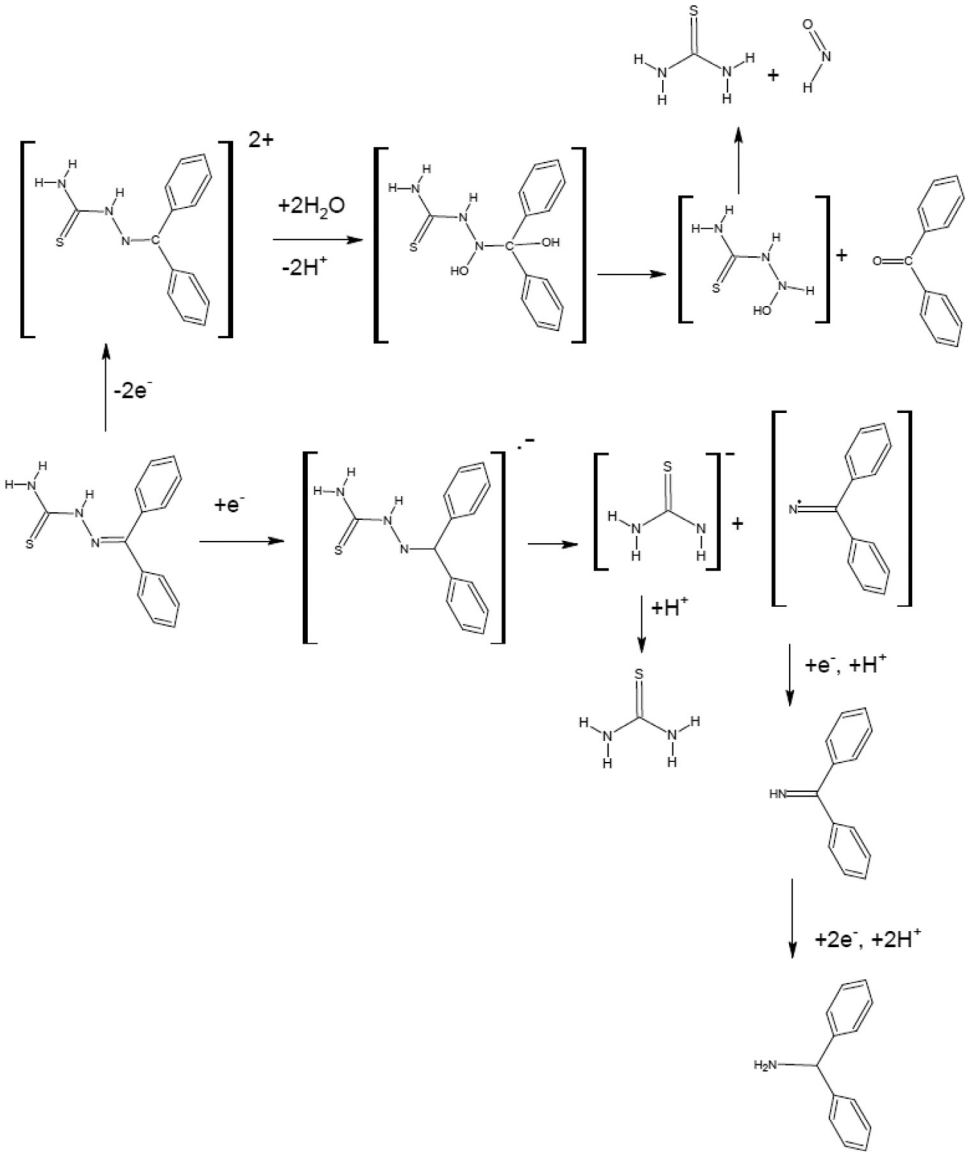

Scheme 2. Plausible mechanisms for the redox decomposition of **1**.

shows irreversible oxidations at $E_{p,a}$ = +1.40 and +1.85 V and electrochemically generated product waves between $E_{p,c}$ = +0.30 and +1.20 V. The closely spaced reduction waves observed between $E_{p,c}$ = −1.20 to −2.20 V hints to delocalization of electrons and mixed metal-ligand reductions. This is consistent with DFT calculations that show facile delocalization of electron density between the HOMO-LUMO orbitals. Comparison of the reduction potentials of **2** with those of thiones that include benzimidazole-2-thione and its derivatives suggests the first reduction wave is due to [C=S] → [C-S]$^{\cdot-}$ [40]. The reduction wave at $E_{p,c}$ = −1.55 V is assigned to $Re^{I/0}$ as it falls in the same region as those observed for *fac*-[$Re(CO)_3$(L-L)Cl] complexes [33,41]. The other reduction waves are ligand-based and can be assigned to [C-S]$^{\cdot-}$ → [C-S]$^{2-}$, [C=N] → [C–N]$^{\cdot-}$ and [C–N]$^{\cdot-}$ → [C–N]$^{2-}$. The oxidation wave at $E_{p,a}$ = +1.40 V is assigned to $Re^{I/II}$ as it fall in the same range as those of $Re^{I/II}$ oxidation in *fac*-[$Re(CO)_3$(L-L)Cl] complexes [21,33]. The multi-electronic oxidation at $E_{p,a}$ = +1.85 V is due to the $2e^-/2H_2O$ decomposition of the 1,1-diphenylmethanimine moiety [N=C($Ph)_2$] to benzophenone. This is similar to those reported for the oxidation of heteroaromatic ketone hydrazonic compounds. When DMF was used in place of CH_3CN similar electrochemical behavior was observed (see supplementary Figure S4). Plausible mechanisms for the electrochemical decomposition of **2** are shown in Scheme 3. The proposed mechanisms are consistent with the observed redox transformations and are similar to those reported for closely related redox transformations in the literature.

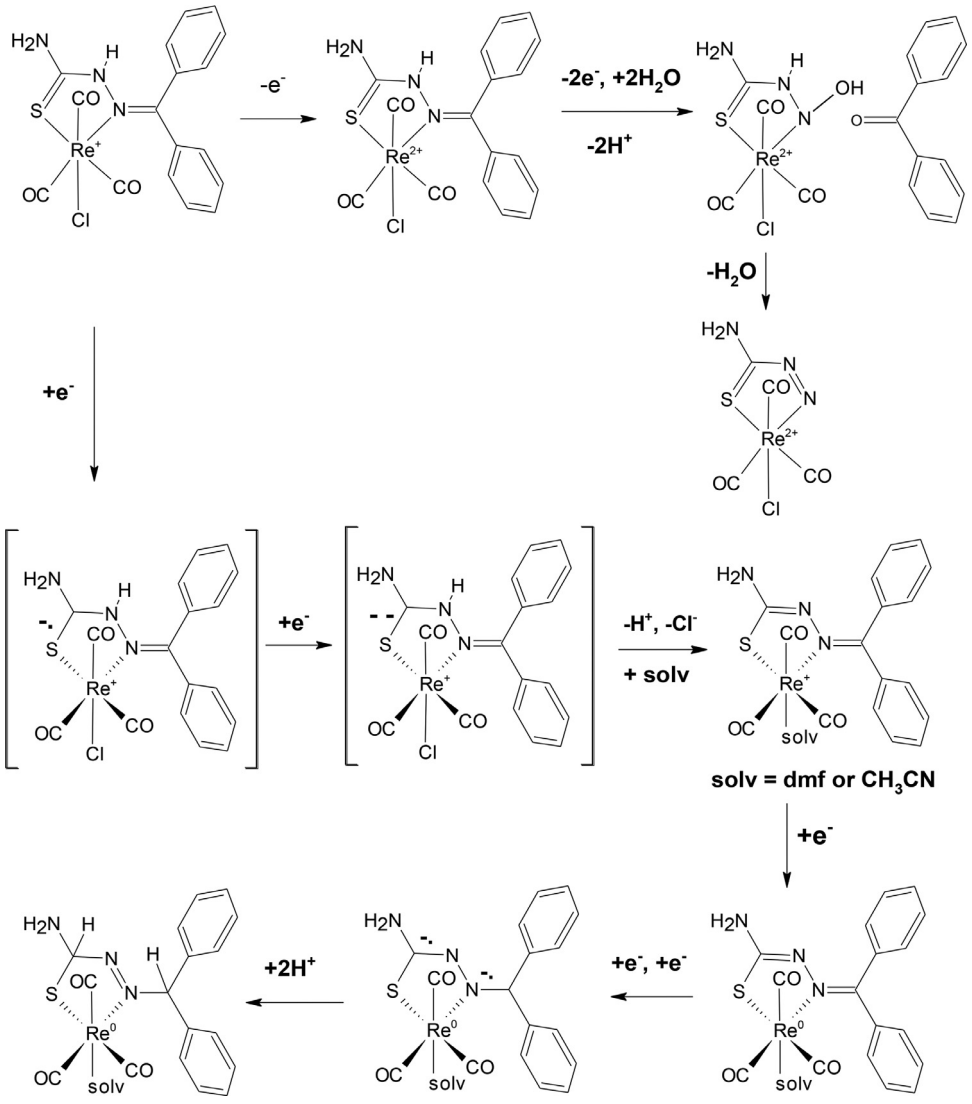

Scheme 3. Plausible mechanisms for the electrochemical decomposition of **2**.

4. Conclusion

fac-[Re(CO)$_3$(κ^2-N$_{im}$,S-bptsc)Cl] isolated from the reaction between Re(CO)$_5$Cl and **1** in toluene displays interesting physicochemical properties. The solid state structure shows the coordination of the thione (C–S) S atom and imine (C–N) N atom of the thioamide group of **1** to Re. The extended structure of **2** shows a network of non-covalent interactions. DFT calculations reveled facile HOMO-LUMO electron transfer. Electrochemical measurements on **1** and **2** in DMF and CH_3CN show sequential irreversible electronic transfers consistent with their electrochemical decomposition. Due to the facile synthesis of hydrazonic compounds, diverse coordination patterns, rich physicochemical properties and applications in various chemical and biological processes, studies are in progress in our laboratory to explore their coordination behavior and molecular sensing and catalytic applications.

Credit author statement

M. B. principal investigator; M. B. and M. A. W. L. designed research; J. J. and M. A. W. L performed synthesis and spectroscopic measurement; M. A. W. L performed electrochemical measurements and DFT calculations; C. M. performed X-ray crystallographic measurements; M. B., M. A. W. L. and C. M. analyzed data; M. B. and M. A. W. L wrote the paper and M. B., M.A. W. L. and C. M. edited the manuscript.

Declaration of Competing Interest

None.

Acknowledgement

The authors express their gratitude to Ms. Shannen Lorraine, Ms. Toni Johnson, and Dr. P. Maragh for their assistance. We are also grateful to The University of the West Indies Mona for financial support.

Supplementary materials

Supplementary material associated with this article can be found, in the online version, at doi:10.1016/j.molstruc.2021.130135.

References

[1] J. Bartoli, S. Montalbano, G. Spadola, D. Rogolino, G. Pelosi, F. Bisceglie, F.M. Restivo, F. Degola, O. Serra, A. Buschini, D. Feretti, C. Zani, M. Carcelli, J. Agri. Food Chem. 67 (2019) 10947–10953, doi:10.1021/acs.jafc.9b01814.

[2] K.G. Sangeetha, K.K. Aravindakshan, Inorg. Chim. Acta 469 (2018) 387–396, doi:10.1016/j.ica.2017.09.057.
[3] R.K. Dubey, S.K. Mishra, A. Mariya, A.K. Mishra, J. Indian Chem. Soc. 90 (2013) 41–48.
[4] R. Chaudhary, Shelly, J. Chem., Biol. Phys. Sci. 2 (2012) 1–5.
[5] K.S.O. Ferraz, N.F. Silva, J.G. Da Silva, N.L. Speziali, I.C. Mendes, H. Beraldo, J. Mol. Struct. 1008 (2012) 102–107, doi:10.1016/j.molstruc.2011.11.035.
[6] S.C. Masikane, S. Mlowe, A.S. Pawar, S.S. Garje, N. Revaprasadu, Russ, J. Inorg. Chem. 64 (2019) 1063–1071, doi:10.1134/s0036023619080072.
[7] P. Paul, P. Sengupta, S. Bhattacharya, J. Organomet. Chem. 724 (2013) 281–288, doi:10.1016/j.jorganchem.2012.11.010.
[8] E.M. Saad, M.S. El-Shahwai, H. Saleh, A.A. El-Asmy, Transition Met. Chem. (Dordrecht, Neth.) 32 (2007) 155–162, doi:10.1007/s11243-006-0138-6.
[9] M. Cabrera, N. Gomez, F. Remes Lenicov, E. Echeverría, C. Shayo, A. Moglioni, N. Fernández, C. Davio, PLoS ONE 10 (2015) e0136878, doi:10.1371/journal.pone.0136878.
[10] A.A. El-Asmy, O.A. El-Gammal, H.S. Saleh, Spectrochim. Acta A Mol. Biomol. Spectrosc. 71 (2008) 39–44, doi:10.1016/j.saa.2007.11.018.
[11] G.D.K. Kumar, G.E. Chavarria, A.K. Charlton-Sevcik, G.K. Yoo, J. Song, T.E. Strecker, B.G. Siim, D.J. Chaplin, M.L. Trawick, K.G. Pinney, Bioorganic Med. Chem. Lett. 20 (2010) 6610–6615, doi:10.1016/j.bmcl.2010.09.026.
[12] S.S.M. Shahriar, H.M. Zakir, M. Jesmin, S.M.M. Ali, Int. J. Biosci. 12 (2018) 111–118, doi:10.12692/ijb/12.1.111-118.
[13] N. Moorthy, P.C. Jobe Prabakar, S. Ramalingam, S. Periandy, K. Parasuraman, J. Mol. Struct. 1110 (2016) 162–179, doi:10.1016/j.molstruc.2016.01.046.
[14] C. Ravikumar, I.H. Joe, J. Raman Spectrosc. 42 (2011) 815–824, doi:10.1002/jrs.2788.
[15] J.L. Ferrer-Herranz, D. Pérez-Bendito, Anal. Chim. Acta 132 (1981) 157–164, doi:10.1016/S0003-2670(01)93886-3.
[16] F. Toribio, J.M. López Fernandez, D.P. Bendito, M. Valcárcel, Microchem. J., 25 (1980) 338–347, doi:10.1016/0026-265X(80)90273-8.
[17] G.E. Chavarria, M.R. Horsman, W.M. Arispe, G.D.K. Kumar, S.-.E. Chen, T.E. Strecker, E.N. Parker, D.J. Chaplin, K.G. Pinney, M.L. Trawick, Eur. J. Med. Chem. 58 (2012) 568–572, doi:10.1016/j.ejmech.2012.10.039.
[18] M. Bakir, I. Hassan, O. Green, J. Mol. Struct. 657 (2003) 75–83, doi:10.1016/S0022-2860(03)00385-5.
[19] M. Bakir, M.W. Lawrence, M. Bohari Yamin, Inorg. Chim. Acta 507 (2020) 119592, doi:10.1016/j.ica.2020.119592.
[20] M. Bakir, M.A.W. Lawrence, P.N. Nelson, R.R. Conry, Electrochim. Acta 212 (2016) 1010–1020, doi:10.1016/j.electacta.2016.07.051.
[21] M. Bakir, J.A.M. McKenzie, J. Chem. Soc. (1997) 3571–3578 Dalton Trans., doi:10.1039/A608470B.
[22] W.L.F. Armarego, C.L.L. Chai, in: Chapter 4 - Purification of Organic Chemicals, Purification of Laboratory Chemicals, 5th edn., Butterworth-Heinemann, Burlington, 2003, pp. 80–388.
[23] M.S. Gordon, M.W. Schmidt, Chapter 41 - Advances in electronic structure theory: GAMESS a decade later, in: C.E. Dykstra, G. Frenking, K.S. Kim, G.E. Scuseria (Eds.), Theory and Applications of Computational Chemistry, Elsevier, Amsterdam, 2005, pp. 1167–1189.
[24] M.W. Schmidt, K.K. Baldridge, J.A. Boatz, S.T. Elbert, M.S. Gordon, J.H. Jensen, S. Koseki, N. Matsunaga, K.A. Nguyen, S. Su, T.L. Windus, M. Dupuis, J.A. Montgomery Jr, J. Comput. Chem. 14 (1993) 1347–1363, doi:10.1002/jcc.540141112.
[25] S.C. Lorraine, M.A.W. Lawrence, M. Celestine, A.A. Holder, J. Mol. Struct. 1222 (2020) 128829, doi:10.1016/j.molstruc.2020.128829.
[26] V.A. Rassolov, J.A. Pople, M.A. Ratner, T.L. Windus, J. Chem. Phys. 109 (1998) 1223–1229, doi:10.1063/1.476673.
[27] A.V. Marenich, C.J. Cramer, D.G. Truhlar, J. Phys. Chem. B 113 (2009) 6378–6396, doi:10.1021/jp810292n.
[28] B.M.Bode, M.S.Gordon, J.Mol. Graphics and Modeling, 16 (1999) 133–138.doi:10.1016/S1093-3263(99)00002-9
[29] C.C. Lovallo, M. Klobukowski, J. Comput. Chem. 25 (2004) 1206–1213, doi:10.1002/jcc.20044.
[30] C.C. Lovallo, M. Klobukowski, J. Comput. Chem. 24 (2003) 1009–1015, doi:10.1002/jcc.10251.
[31] G.M. Sheldrick, Acta Crystallogr., Sect. C: Struct. Chem. 71 (2015) 3–8, doi:10.1107/S2053229614024218.
[32] M. Bakir, M.B. Yamin, J. Coord. Chem. 72 (2019) 3657–3673, doi:10.1080/00958972.2019.1696961.
[33] M. Bakir, J. Electroanal. Chem. 466 (1999) 60–66, doi:10.1016/S0022-0728(99)00122-9.
[34] M. Bakir, K. Abdur-Rashid, Transition Met. Chem. 24 (1999) 384–388, doi:10.1023/A:1006997111108.
[35] L.A. Paul, N.C. Roettcher, J. Zimara, J.-.H. Borter, J.-.P. Du, D. Schwarzer, R.A. Mata, I. Siewert, Organometallics 39 (2020) 2405–2414, doi:10.1021/acs.organomet.0c00240.
[36] D.M. Wiles, B.A. Gingras, T. Suprunchuk, Can. J. Chem. 45 (1967) 469–473, doi:10.1139/v67-081.
[37] G. Habarurema, E.C. Hosten, R. Betz, T.I.A. Gerber, Inorg. Chem. Commun. 47 (2014) 159–161, doi:10.1016/j.inoche.2014.07.042.
[38] M. Bakir, Acta Crystallogr., Sect. C: Cryst. Struct. Commun. C58 (2002) m74–m76, doi:10.1107/S0108270101019527.
[39] M. Bakir, Acta Crystallogr., Sect. C: Cryst. Struct. Commun. C57 (2001) 1371–1373, doi:10.1107/S0108270101013890.
[40] T. Zhang, J. Wang, Z. Tai, S. Zhu, J. Electroanal. Chem. 393 (1995) 55–59, doi:10.1016/0022-0728(95)03947-F.
[41] M. Bakir, J.A.M. McKenzie, J. Electroanal. Chem. 425 (1997) 61–66, doi:10.1016/S0022-0728(96)04940-6.